AdvWarp: A Transformation Algorithm for Advanced Modeling of Gas Compressors and Drives

Anton Baldin[1], Kläre Cassirer[1], Tanja Clees[1,2], Bernhard Klaassen[1], Igor Nikitin[1], Lialia Nikitina[1] and Sabine Pott[1]

[1]*Fraunhofer Institute for Algorithms and Scientific Computing, Schloss Birlinghoven, 53754 Sankt Augustin, Germany*

[2]*Bonn-Rhine-Sieg University of Applied Sciences, Grantham-Allee 20, 53754 Sankt Augustin, Germany*

Anton.Baldin, Klaere.Cassirer, Tanja.Clees, Bernhard.Klaassen, Igor.Nikitin, Lialia.Nikitina, Sabine.Pott

Keywords: Complex Systems Modeling and Simulation, Non-linear Systems, Applications in Energy Transport.

Abstract: Solving transport network problems can be complicated by non-linear effects. In the particular case of gas transport networks, the most complex non-linear elements are compressors and their drives. They are described by a system of equations, composed of a piecewise linear 'free' model for the control logic and a non-linear 'advanced' model for calibrated characteristics of the compressor. For all element equations, certain stability criteria must be fulfilled, providing the absence of folds in associated system mapping. In this paper, we consider a transformation (warping) of a system from the space of calibration parameters to the space of transport variables, satisfying these criteria. The algorithm drastically improves stability of the network solver. Numerous tests on realistic networks show that nearly 100% convergence rate of the solver is achieved with this approach.

1 INTRODUCTION

In this paper, we continue the construction of globally converging solver algorithm for stationary transport network problems. The approach is based on conditions of generalized resistivity formulated in our previous work (Clees et al., 2018a). Specifically for the natural gas transport, the modeling of key elements, the compressors, combines two parts, identified in gas simulation community as 'free' and 'advanced' models. The 'free' model represents the control logic of compressors, related to the fulfillment of goals, such as the input/output pressure or flow. The 'advanced' model describes the individual physical characteristics of compressors determined by calibration procedure. The construction of the algorithm for advanced modeling of compressors was started in (Clees et al., 2018b), continued in (Baldin et al., 2020), and further improved in the present paper.

The advanced model of compressors and drives considers the space of calibration parameters such as volumetric flow, revolution number, as well as various energy characteristics. Although the representation of compressors and drives in this space is more convenient for calibration, for solving transport network problems it is more suitable to represent them in the space, describing the main transport characteristics, such as inlet and outlet pressures and mass flow. It is important to fulfill the conditions of generalized resistivity (Clees et al., 2018a), which means that the flow must be an increasing function of the inlet pressure and a decreasing function of the outlet pressure. For the global convergence of the solver, this condition must be satisfied everywhere, including the exterior of the working region, since the solver can wander around there during the iterations.

In this work, to construct the element equation, an improved pixel algorithm from (Clees et al., 2018b) is used. A triangular grid (Baldin et al., 2020) is implemented, which can be adaptively compressed in places where higher resolution is required. Warping of the grid will be performed in the solution loop whenever the temperature or/and the gas composition change. This approach provides a simple control over the system resistivity by calculating the normals to the triangles. We tested the method on a variety of realistic examples and obtained nearly 100% convergence of the solver. The approach enhances our multi-physics network simulator MYNTS (Clees et al., 2016).

Modeling of gas transport networks has been described in detail in works (Mischner et al., 2011;

Baldin, A., Cassirer, K., Clees, T., Klaassen, B., Nikitin, I., Nikitina, L. and Pott, S.
AdvWarp: A Transformation Algorithm for Advanced Modeling of Gas Compressors and Drives.
DOI: 10.5220/0010512602310238
In *Proceedings of the 11th International Conference on Simulation and Modeling Methodologies, Technologies and Applications (SIMULTECH 2021)*, pages 231-238
ISBN: 978-989-758-528-9

Schmidt et al., 2015). The most numerous elements in such networks are pipes, represented by a non-linear friction law. In this law, the main dependence is quadratic, and empirical approximations by Nikuradse, Hofer, or Colebrook-White (Nikuradse, 1950; Colebrook and White, 1937) are typically used. The gas pressure and density are related by the equation of state, for which also different approximations exist; commonly used are Papay, AGA8-DC92, GERG-2008 (Saleh, 2002; CES, 2010; Kunz and Wagner, 2012). The balance of flows is described by linear Kirchhoff equations. Finally, all the equations are collected in a large non-linear system, which can be considered as a particular type of non-linear program (NLP). It can be solved by standard NLP solvers, such as IPOPT, SNOPT, MINOS (Wächter and Biegler, 2006; Gill et al., 2005; Murtagh and Saunders, 1978). Our simulator also features an own solver, implementing a stabilized Newton's method with Armijo's rule (Kelley, 1995).

This paper is organized as follows. In Section 2 the transformation algorithm from the space of calibration parameters to the space of transport variables is presented. In Section 3 tests of the algorithm on a number of realistic gas transport networks are described and analyzed. In Section 4 the obtained results are summarized.

2 THE ALGORITHM

In the following, the general strategy as well as decisive details of the novel algorithm are introduced.

Strategy: for stable representation of advanced compressors and drives is based on the following steps:

- eliminate all intermediate variables in the element equation;
- represent the equation in the space of transport variables;
- check monotonicity;
- use a monotone linear continuation outside of the working region.

The sets of variables and the transformation between them will be described further. The monotonicity condition is required for global convergence of the solver algorithm and is described in (Clees et al., 2018a). All element equations $f(P_{in}, P_{out}, Q) = 0$ should satisfy the following inequalities on their derivatives:

$$\partial f/\partial P_{in} > 0,\ \partial f/\partial P_{out} < 0,\ \partial f/\partial Q < 0, \quad (1)$$

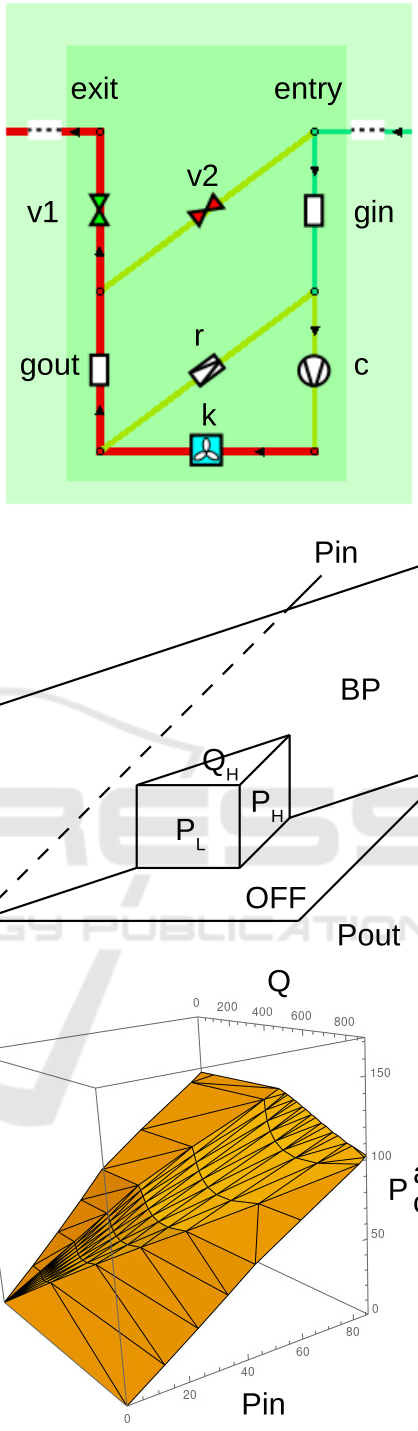

Figure 1: Modeling of compressors. On the top: the structure of compressor station. In the center: compressor element equation in transport variables, 'free' model. On the bottom: 'advanced' model. Images from (Clees et al., 2018a; Clees et al., 2018b; Baldin et al., 2020).

meaning that the element equation function should monotonously increase w.r.t. P_{in} and monotonously

decrease w.r.t. P_{out}, Q.

The basic continuation formula is also presented in (Clees et al., 2018a):

$$\begin{aligned} &f(x_1,...,x_n) = f(\hat{x}_1,...,\hat{x}_n) \\ &+\sum_{k=1}^{n}(\min(x_k-a_k,0)+\max(x_k-b_k,0)), \quad (2) \\ &\hat{x}_k = \min(\max(x_k,a_k),b_k). \end{aligned}$$

It provides a continuation of the function of n arguments, monotonously increasing w.r.t. every argument, from a bounding box specified by $[a_k,b_k]$ limits to the whole space, preserving this monotonous property. For decreasing functions, coordinate reflections can be used.

Structure: of the compressor station in its typical one-unit configuration is shown in Figure 1 top. It consists of the following elements: c – compressor, r – bypass regulator, gin/gout – input and output resistors, v1,2 – main and bypass valves, k – cooler. Entry/exit identify standard input and output nodes. In more complicated scenarios several units can be assembled together in parallel or/and serial connection.

Transport Variables: Figure 1 center and bottom show the element equation of compressor in the space of transport variables. $P_{in,out}$ denote input and output pressures, normally measured in bars. Q is a throughput, standardly represented by mass flow Q_m in kg/s. With the known gas composition it can be converted to molar flow Q_v in mol/s, or to normal flow Q_N in cubic meters of gas virtually decompressed to normal pressure and temperature, per second (often re-expressed to thousands of such normal cubic meters per hour). Special case is volumetric flow Q_{vol}. It is measured in m^3/s at current conditions, and due to compressibility of the gas depends on whether input or output conditions are meant (input conditions are taken by default).

Figure 1, central image, presents the free model. The subscripts H, L indicate high and low control settings, defining upper and lower limits on the pressures and the flow; BP is open/bypass mode of compressor $P_{in} = P_{out}$; OFF is the closed mode $Q = 0$. This polyhedral surface, as all surfaces of this kind, can be represented by max-min formula:

$$\begin{aligned} &\max(\min(\ P_{in}-P_L, -P_{out}+P_H, -Q+Q_H), \quad (3) \\ &P_{in}-P_{out}, -Q)+\varepsilon(P_{in}-P_{out}-Q)=0, \end{aligned}$$

where the last term with small positive constant ε serves regularization.

Figure 1 bottom presents advanced compressor model. $P^{adv}_{out}(P_{in},Q)$ is output pressure of compressor in the absence of control restrictions (also referred as compressor in MAX mode). It is considered as a function of the input pressure and the flow. This function represents the internal capability of compressor and its drive. It is combined with free diagram as follows:

$$\begin{aligned} &\max(\min(\ P_{in}-P_L, -P_{out}+P_H, -Q+Q_H, \\ &-P_{out}+P^{adv}_{out}(\hat{P}_{in},\hat{Q}) \\ &+\min(P_{in}-P^{adv}_{in,min},0)+\max(P_{in}-P^{adv}_{in,max},0) \\ &+\min(-Q+Q^{adv}_{max},0)+\max(-Q+Q^{adv}_{min},0) \quad (4) \\ &),P_{in}-P_{out},-Q)+\varepsilon(P_{in}-P_{out}-Q)=0, \\ &\hat{P}_{in}=\min(\max(P_{in},P^{adv}_{in,min}),P^{adv}_{in,max}), \\ &\hat{Q}=\min(\max(Q,Q^{adv}_{min}),Q^{adv}_{max}), \end{aligned}$$

here the second line represents the advanced surface, inserted into the free formula; the next two lines provide linear continuation of this surface outside of the bounding box; the last two lines define clamp functions to the bounding box.

The advanced surface is triangulated, every triangle is represented by own system of barycentric coordinates. For this purpose, on the plane $(P_{in},Q)=(x,y)$ the vertices of triangle $\{v_1,v_2,v_3\}$ are defined. The point on triangle is then defined as $\sum_i w_i v_i = (x,y)$, $\sum_i w_i = 1$. The system can be solved for the weights $w_i(x,y)$ by linear formulae $w_i(x,y) = c_{0i}+c_{xi}x+c_{yi}y$, with 3 constants (c_{0i},c_{xi},c_{yi}) per w_i precomputed. One formula can be spared using $w_3 = 1-w_1-w_2$. The point belongs to triangle, when all weights are non-negative $w_i \geq 0$.

The third coordinate $P_{out} = z$ is found by one more linear formula $z(x,y) = \sum_i w_i(x,y) z_i$. Altogether 9 coefficients (equivalent to 3 nodes x 3 coordinates) are precomputed. Explicit lengthy formulae for barycentric coordinates can be found in (Baldin et al., 2020). Finally, a function is implemented, searching for a triangle on xy-plane and evaluating z-coordinate and its xy-derivatives. The derivatives can be directly used to check monotonicity condition:

$$\begin{aligned} &-P_{out}+P^{adv}_{out}(P_{in},Q)=0, \quad (5) \\ &\partial P^{adv}_{out}/dP_{in}>0,\ \partial P^{adv}_{out}/dQ<0. \end{aligned}$$

Equivalently, these conditions can be reformulated in terms of normals to triangles, which all should point to the octant $(P_{in},P_{out},Q)=(+,-,-)$.

Internal Variables: Density ρ is defined as monotonously increasing function of pressure P using equations of state (EOS), involving also the molar mass μ, the temperature T and the compressibility factor z. Different analytic or numerical EOS can be used, e.g., Papay (Saleh, 2002), AGA8-DC92

(CES, 2010), GERG-2008 (Kunz and Wagner, 2012). The volumetric flow relative to input conditions is expressed via mass flow and density as $Q_{vol} = Q/\rho_{in}$. The revolution number *rev* and torque M_t describe the rotation of the engine. There are also energetic quantities characterizing compressors and drives: H_{ad} – increase of adiabatic enthalpy, η_{ad} – adiabatic efficiency, *Perf* – performance power.

Transformation: consists of a sequence of nonlinear maps:

$$(Q_{vol}, rev) \xrightarrow{1} (H_{ad}, \eta_{ad}, Perf_{max}) \xrightarrow{2} \\ \rightarrow (\rho_{in}, H_{ad}, Q) \xrightarrow{3} (P_{in}, P_{out}, Q). \quad (6)$$

Step 1: standard 1D quadratic and 2D biquadratic models from (Clees et al., 2018b):

$$H_{ad} = (1, rev, rev^2) \cdot A \cdot (1, Q_{vol}, Q_{vol}^2)^T, \\ \eta_{ad} = (1, rev, rev^2) \cdot B \cdot (1, Q_{vol}, Q_{vol}^2)^T, \quad (7) \\ Perf_{max} = (1, rev, rev^2) \cdot D^T,$$

where A, B are constant 3x3 matrices and D is a constant 3-vector filled by calibration coefficients. $Perf_{max}$ is the maximal performance power provided by the drive at the given revolution number.

Step 2: temperature and gasmix independent models:

$$Q = Perf_{max}\eta_{ad}/H_{ad}, \ \rho_{in} = Q/Q_{vol}, \quad (8)$$

Step 3: temperature and gasmix dependence:

$$\alpha = (\kappa - 1)/\kappa, \ \gamma = RT_{in}/\mu, \\ P_{in} = EOS_{inv}(\rho_{in}), \ z_{in} = P_{in}/(\gamma\rho_{in}), \quad (9) \\ P_{out} = P_{in}(H_{ad}\alpha/(\gamma z_{in}) + 1)^{1/\alpha},$$

where κ is the adiabatic exponent, R is universal gas constant; the equation of state $\rho = EOS(P)$ is inverted to define P_{in}; the universal gas law $P = \rho RTz/\mu$ is resolved w.r.t. z; then H_{ad} definition from (Clees et al., 2018b) is resolved w.r.t. P_{out}.

All equations are given in SI-units, practically conversion factors should be applied for the transformations W/kW/MW, bar/Pa etc.

Regions: of the advanced surface are shown in Figure 2 top. The described transformations are used to construct the most important powmax region, where the performance of compressor is restricted solely by the power of its drive. It is bounded by *revmin*/*revmax* lines and $Q_{vol,min}/\eta_{min}$ lines (also called surge line and choke line). Here *revmin* and

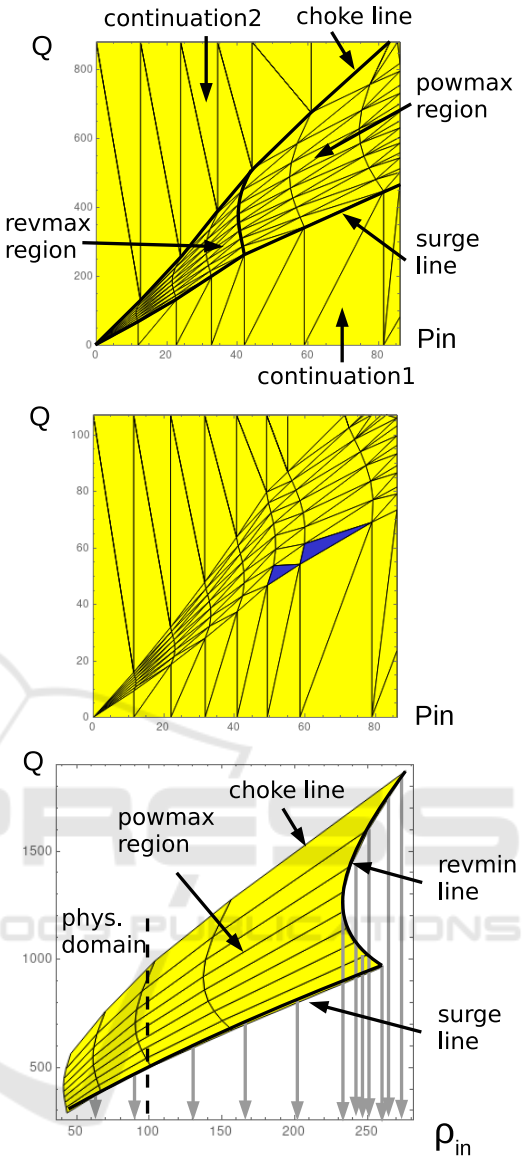

Figure 2: Details of compressor diagrams. On the top: regions of the advanced surface in (P_{in}, Q) projection. In the center: problems with monotonicity detected (blue triangles). On the bottom: the fold on *revmin* line.

revmax are given constants. Surge line is defined as

$$Q_{vol,min}(rev) = \max(Q^{(1)}_{vol,min}, Q^{(2)}_{vol,min}, 0), \\ Q^{(1)}_{vol,min} = (1, rev, rev^2) \cdot C^T, \quad (10) \\ Q^{(2)}_{vol,min} = \arg\max_{Qvol} H_{ad}(Q_{vol}, rev),$$

$Q^{(1)}_{vol,min}$ is given as 1D quadratic model with a calibration 3-vector C; the condition $Q_{vol} \geq Q^{(2)}_{vol,min}$ defines a physical decreasing branch of quadratic dependence of H_{ad} on Q_{vol} at fixed *rev*; the outflow

condition $Q_{vol} \geq 0$ is also enforced. Choke line $\eta_{ad}(Q_{vol,max}, rev) = \eta_{min}$ with a given constant η_{min} is solved w.r.t. $Q_{vol,max}(rev)$. Generally it is a quadratic equation with two roots; the maximal root is taken. The region between $revmin/revmax$ and surge/choke lines is resampled to $N_{rev} \times N_\eta$ grid.

Revmax region: $rev = revmax$ side is taken and in (ρ_{in}, Q) projection proportionally scaled to the origin. Then it is mapped to the final (P_{in}, Q) coordinates by the inverse EOS transformation above.

Continuation regions 1 and 2 go downwards and upwards in the (ρ_{in}, Q) projection, respectively, till the limits of the bounding box. H_{ad} values in these continuations are kept constant.

P_{out}-coordinate in (9) lifts the whole construction to 3D space (P_{in}, P_{out}, Q), where the final surface is represented by triangulation. Orientation of normals allows to check monotonicity conditions for every triangle. Figure 2 center indicates problems with monotonicity (blue triangles). These problems happen rarely and require a slight local adjustment of the diagram to satisfy the global convergence criterion.

In general, the revmin side of the powmax patch has a fold, shown in Figure 2 bottom. Physically, on the surge and revmin lines, a bypass regulator opens in compressor station (r in Figure 1 top). It redirects a part of the flow to circulate through the compressor, preventing the compressor from going outside of the working region ($Q_{vol} < Q_{vol,min}$, $rev < revmin$). In our diagrams, total Q passing through the compressor and its bypass regulator is continued downwards from these lines. This continuation generally creates a fold, producing multiple solutions and degeneracy of the Jacobi matrix. Fortunately, for most of the cases, this fold is located beyond the physical domain of ρ_{in} or P_{in} and can be safely ignored. For extra safety, we define a $\rho_{in,max}$ value, cutting off the fold and restricting the patch by this value.

The other problematic case is displayed in Figure 3 top. It corresponds to the increasing torque dependence $M_t(rev) = Perf_{max}/rev$. If the drive is joined with a generic resistive load, $M_{t,sys}(rev) = c_0 + c_1 rev$ for dry and viscous friction, or other increasing $M_{t,sys}(rev)$ dependence, the stable intersection is ensured only when $M_{t,drive}(rev)$ is decreasing, Figure 3 center. Otherwise one can find such resistive system that none or multiple intersections exist, Figure 3 bottom. In this case multiple solutions or no solution exist for the whole network problem. Such problematic behavior is present in some electric engines (E-drives). The computations show that in this case the monotonicity conditions are violated in most of the diagram. The solution we have taken so far is to replace the actual $M_{t,drive}(rev)$ dependence with

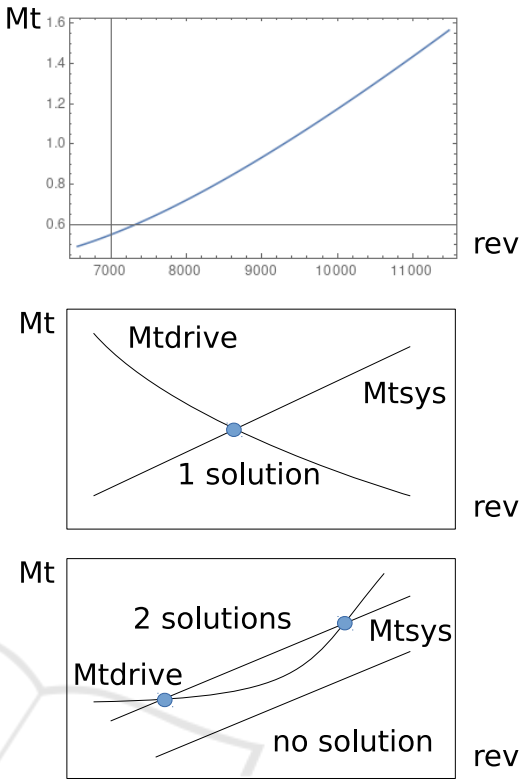

Figure 3: Dependence of torque on revolution number. On the top: problematic case with increasing $M_t(rev)$ dependence. In the center: stable intersection of increasing $M_{t,sys}(rev)$ and decreasing $M_{t,drive}(rev)$. On the bottom: no intersection or multiple intersections for increasing $M_{t,drive}(rev)$.

a weakly decreasing function that limits the real dependence from below (conservative), above (overestimation), or reproduces it on average. In practice, a constant $M_{t,drive}$ can be used here, since the regularization in the control equation removes all marginal degenerations in the system.

The described transformation procedure is applied sequentially for all compressor-drive pairs in the network, as shown in Figure 4. Steps 1 and 2 of the transformation are performed once, in precomputation mode. The monotonous decrease of $M_t(rev)$, regularity of surge and choke lines, absence of folds on 2D diagrams is visually controlled. Step 3 of the transformation is applied repeatedly during the solution procedure, every time when the temperatures or/and gas composition changes. This step is just a monotonous remapping $\rho_{in} \to P_{in}$ according to the current EOS, not violating the verified monotonicity conditions.

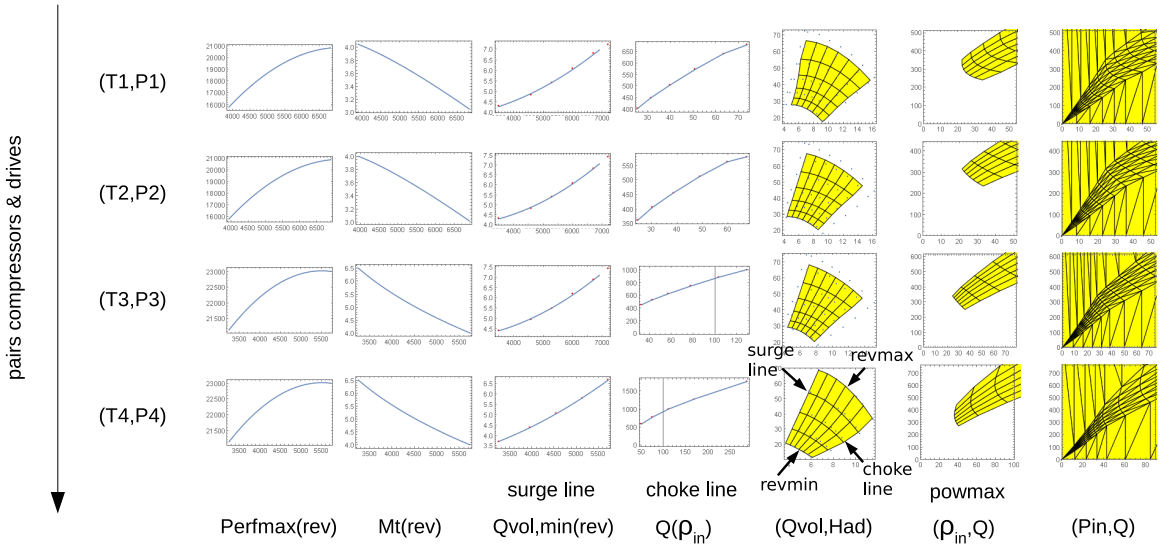

Figure 4: Construction of advanced representation for all compressor-drive pairs in the network.

Station Resistors: shown by gin/gout in Figure 1 top, the resistors typically support constant pressure drops (REPD) on entry and exit of compressor station. They lead to trivial modification of the control equation (4), where in the first line $P_{in/out}$ represent the pressure in entry/exit nodes, while in the rest of the formula $P_{in/out}$ are replaced with the pressure at inlet/outlet of the compressor. These values differ by the given pressure drops on station resistors.

Ambient Temperature Dependence: compressor drives often possess an own dependence on ambient temperature, defined by biquadratic model:

$$Perf_{max} = (1, rev, rev^2) \cdot D \cdot (1, T_{amb}, T_{amb}^2)^T, \quad (11)$$

used instead of (7). Here D is 3x3 calibration matrix and T_{amb} is absolute or relative temperature, with the corresponding recomputation. Note that the actual use of $Perf_{max}$ in step 2 of the transformation is a linear formula (8). As a result, the following linear algorithm can be used for precise account of T_{amb}-dependence. The step 2 precomputation is performed for three different temperature values $T_{amb,i}$, producing three 2-vectors $v_i = (\rho_{in}, Q)_i$. Then, in step 3, three weights are computed, defined by

$$w_1 = \frac{(T_{amb} - T_{amb,2})(T_{amb} - T_{amb,3})}{(T_{amb,1} - T_{amb,2})(T_{amb,1} - T_{amb,3})} \quad (12)$$

and the cyclic permutation of indices. Then the vector v is computed as the weighted average $v = \sum_i w_i v_i$ and the result is passed to step 3 of the generic computation. In this way, the variation of T_{amb} in particular scenario can be performed without repeating the steps1,2 in the chain.

3 NUMERICAL TESTS

The described algorithm has been tested on a number of real-life gas networks. Parameters of the test networks are given in Table 1. The number of elements is given before applying topological cleaning procedure, described in (Clees et al., 2018b). This procedure removes trivial elements, such as valves, shortcuts, short pipe segments, and can significantly reduce the size of the network in certain cases. While the transport networks mainly consist of pipes with a nearly quadratic friction law, their computational complexity is defined by the most non-linear elements, namely compressors and regulators. In the networks, there are two types of supply nodes, the ones with a pressure setpoint ($Pset$) and the ones with an inflow setpoint ($Qset < 0$). Many outflow nodes ($Qset > 0$) exist, representing the large number of gas consumers in the network.

The small and medium size networks are presented in Figure 5. Network N1 has 100 nodes and 111 edges, while ME has 437 nodes and 482 edges and possesses a more complex topology. In addition, we use a set of 85 large networks received from our industrial partner for benchmarking. They are subdivided to L- and H-type denoting gas with low and high calorific value. Although the calorific value itself has no influence on the convergence properties, the L-networks contain considerably less compressors and are topologically more simple than their H-counterparts. As a result, L-networks typically possess better convergence then the H-ones.

The test networks were subjected to the solver procedures of two types. One used the ‘old’ type

Table 1: Parameters of test networks.

network	nodes	edges	pipes	compressors	regulators	Psets	Qsets
N1	100	111	34	4	4	2	3
ME	437	482	370	20	24	3	164
N85/L	3232-3886	3305-3974	2406-2835	1-7	59-77	6-7	625-843
N85/H	2914-3818	2989-3952	1498-1937	16-42	59-107	5-9	328-505

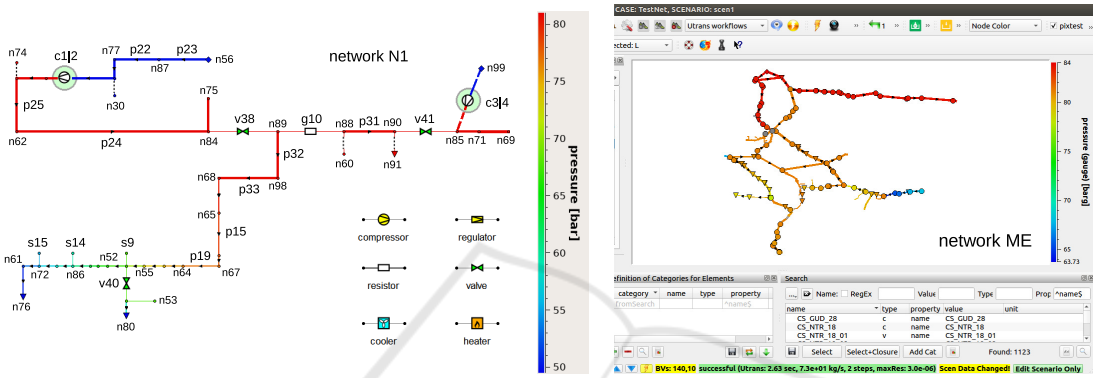

Figure 5: Test networks N1 and ME.

of the compressor modeling, where all intermediate variables were present and constrained by the corresponding equations. The other one used the 'new' type, with intermediate variables eliminated and the problem formulated completely in terms of the transport variables. The convergence results are shown in Table 2. While the old procedure was sufficiently stable to process simple N1 and ME networks, as well as L-type N85 networks, it diverged in the half of H-type N85 networks. Our main achievement is that the new procedure converged in our tests in 100% of cases, also in the most complex N85/H-type ones.

It should be noted, however, that in spite of the theoretical guarantee for the convergence of the algorithm, the control equations (3) and (4) contain problematic marginally degenerate terms. They correspond to the faces of the 'free' diagram (Figure 1, center), with normals directed exactly along coordinate axes. On such faces, some derivatives in (1) vanish and the whole network problem degenerates. Regularizing the ε-term in the control equations formally removes this singularity. However, precise physical modeling requires ε to be as small as possible while for numerical stability larger values of ε are preferable. In our applications, a compromise value in the range $\varepsilon = [10^{-6}, 10^{-3}]$ is selected.

As a result of the marginally singular problem statement, the solution procedure cannot be started

Table 2: Results.

test networks	total num.	converged old	converged new
N1	1	1	1
ME	1	1	1
N85/L	23	23	23
N85/H	62	31	62

from an arbitrary point, as it should be possible for the absolutely stable globally convergent algorithm. It still requires empirics in the definition of a starting point, for which we use a 'gradual sophistication' strategy. It starts from 'forced' goals of compressors and regulators and proceeds via 'free' to 'advanced' modeling. We have found that the solution procedure can randomly diverge under variations of the problem settings. It happens rarely, by our experience in $\sim 1\%$ of cases. In these special cases the adjustment of ε value, global per network or local per problematic element, may help.

4 CONCLUSIONS

In this paper, the advanced modeling of gas compressors and their drives is considered. The approach is based on the transformation of a system from the space of calibration parameters to the space of transport variables. In the solution loop, the transformation is readjusted whenever the temperature or/and the gas composition in the network change. The transformation satisfies stability criteria providing the global convergence of the solution procedure. For the 87 test cases considered, 100% convergence rate is achieved.

The remaining problem is the presence of the marginally degenerate terms in the control equation of compressors and regulators. In our current approach, we regularize these terms with a small positive parameter, whose value is balanced between physical precision and numerical stability of the modeling. Other approaches have to be tested, in particular, enhancing the system by dynamic behavior and studying the stability of the integrator of the corresponding system of differential algebraic equations.

Our further plans also include the consideration of 'generic' modeling, intermediate between 'free' and 'advanced', as well as a special analytically solvable case of piston compressors.

ACKNOWLEDGMENT

We acknowledge the support of the German Federal Ministry for Economic Affairs and Energy, project BMWI-0324019A, MathEnergy: Mathematical Key Technologies for Evolving Energy Grids.

REFERENCES

Baldin, A. et al. (2020). Topological Reduction of Stationary Network Problems: Example of Gas Transport. *International Journal On Advances in Systems and Measurements*, 13:83–93.

CES (2010). *DIN EN ISO 12213-2: Natural gas – Calculation of compression factor*. European Committee for Standardization.

Clees, T. et al. (2016). MYNTS: Multi-phYsics NeTwork Simulator. In *SIMULTECH 2016, July 29–31, 2016, Lisbon, Portugal*, pages 179–186. SCITEPRESS.

Clees, T. et al. (2018a). Making Network Solvers Globally Convergent. *Advances in Intelligent Systems and Computing*, 676:140–153.

Clees, T. et al. (2018b). Modeling of Gas Compressors and Hierarchical Reduction for Globally Convergent Stationary Network Solvers. *International Journal On Advances in Systems and Measurements*, 11:61–71.

Colebrook, C. F. and White, C. M. (1937). Experiments with Fluid Friction in Roughened Pipes. *Mathematical and Physical Sciences*, 161:367–381.

Gill, P. E. et al. (2005). SNOPT: An SQP algorithm for large-scale constrained optimization. *SIAM Review*, 47(1):99–131.

Kelley, C. T. (1995). *Iterative Methods for Linear and Nonlinear Equations*. SIAM, Philadelphia.

Kunz, O. and Wagner, W. (2012). The GERG-2008 wide-range equation of state for natural gases and other mixtures: An expansion of GERG-2004. *J. Chem. Eng. Data*, 57:3032–3091.

Mischner, J. et al. (2011). *Systemplanerische Grundlagen der Gasversorgung*. Oldenbourg Industrieverlag GmbH.

Murtagh, B. and Saunders, M. (1978). Large-scale linearly constrained optimization. *Mathematical Programming*, 14:41–72.

Nikuradse, J. (1950). *Laws of flow in rough pipes*. NACA Technical Memorandum 1292, Washington.

Saleh, J. (2002). *Fluid Flow Handbook*. McGraw-Hill.

Schmidt, M. et al. (2015). High detail stationary optimization models for gas networks: model components. *Optimization and Engineering*, 16(1):131–164.

Wächter, A. and Biegler, L. T. (2006). On the implementation of an interior-point filter line-search algorithm for large-scale nonlinear programming. *Mathematical Programming*, 106(1):25–57.